Theory of effective g-factors in ternary semiconductors: application to $Pb_{1-x}Sn_xTe$

1991 J. Phys.: Condens. Matter 3 6299

(http://iopscience.iop.org/0953-8984/3/33/009)

J. Phys.: Condens. Matter 3 (1991) 6299–6311. Printed in the UK

Theory of effective g-factors in ternary semiconductors: application to $Pb_{1-x}Sn_xTe$

R L Hota and G S Tripathi
Department of Physics, Berhampur University, Berhampur 760007, Orissa, India

Received 27 February 1991.

Abstract. The effective g-factor, obtained from the spin contribution to the Knight shift, is calculated from first principles for ternary semiconductors and applied to $Pb_{1-x}Sn_xTe$. A six-level $k \cdot \pi$ theory, within the framework of the effective-mass representation, is used to calculate the effective g-factor as a function of carrier density, tin concentration and temperature. The temperature and concentration dependence of the energy gap is used via the virtual-crystal approximation. The agreement with the available experiments is good, and the trends and results obtained are in overall conformity with that found in the experiments.

1. Introduction

The calculation of the effective g-factor in semiconductors is important because of the dependence of the Knight shift on this quantity (Tripathi *et al* 1981, 1982). Recently, it has received particular attention in view of its anomalous characteristic in the relatively new semiconductors, namely the semimagnetic semiconductors (Dobrowolska *et al* 1981, Dobrowolski *et al* 1981, Bastard *et al* 1981, Heiman *et al* 1983), where the g-factors are found to be enhanced by two orders of magnitude with reference to the corresponding ordinary semiconductors.

The concept of 'effective spin Hamiltonian' and effective g-factors was first introduced by Roth (1960), who obtained an expression for this factor, considering the antisymmetric part of the g-tensor, noting that the symmetric part vanishes for a crystal with inversion symmetry, Yafet (1963) obtained an expression for the square of the effective g-factor, by considering explicitly the spin–orbit interaction. Misra and Kleinman (1972) derived an expression for the effective Pauli spin susceptibility as a function of the square of the effective g-factor. They have shown the equivalence of their results with that of Yafet (1963). While the effective Pauli spin susceptibility depends on the square of the effective g-factor, the dependence of the Knight shift on the effective g-factor is linear (Tripathi *et al* 1981, 1982, deCastro and Schumacher 1973). Thus, the sign of the g-factor is ascribed from the sign of the Knight shift (Hewes *et al* 1973). Our interest in the effective g-factor in ternary semiconductors, particularly in $Pb_{1-x}Sn_xTe$, is motivated primarily due to the controversy attached to the role and sign of g-factors in the Knight shift of these systems (Leloup and Sapoval 1979). Furthermore, although the band-edge g-factors in PbTe have been discussed by several authors (Mitchell and Wallis 1969, Leloup and Sapoval 1979, Leloup *et al* 1973, Sapoval and Leloup 1973, Bernick and Kleinman 1970), there has been no satisfactory calculation

0953-8984/91/336299 + 13 $03.50

from first principles of the effective g-factors in $Pb_{1-x}Sn_xTe$ as a function of carrier concentration, tin concentration and temperature. This work presents such a calculation, for the first time, and may be viewed as as extension of our calculations of the magnetic properties of these systems (Tripathi *et al* 1981, 1982, Misra *et al* 1984, 1985, 1986, 1987, Misra and Tripathi 1989, Hota and Tripathi 1990).

The organization of the paper is as follows. Section 2 discusses the general expression for the effective g-factor. We discuss in section 3 the effective-mass approximation and the related $\boldsymbol{k}\cdot\boldsymbol{\pi}$ band model as appropriate to $Pb_{1-x}Sn_xTe$. Section 4 presents the results of our calculation followed by a discussion. We summarize the work in section 5 with an appropriate conclusion.

2. General expression for the effective g-factor

As mentioned earlier, the effective g-factor is an integral part of the Knight shift (K_s). The general expression for K_s, in the presence of many-body and spin–orbit effects, is (Tripathi *et al* 1981, 1982)

$$K_s^{\nu\mu} = -\tfrac{1}{2}\mu_B^2 \sum_{n,k,\rho} \frac{1}{1-\alpha_n(k)} X^{\nu}_{n\rho,n\rho'} g^{\mathrm{eff},\mu}_{n,n}(k) f'(E_{nk}) \tag{2.1}$$

where $\alpha_n(k)$ is the exchange-enhancement factor; X is the hyperfine vertex, which includes the contact, dipolar and orbital hyperfine interactions; $f'(E_{nk})$ is the energy derivative of the Fermi function; and $g^{\mathrm{eff},\mu}_{n,n}(k)$ is the intra-band effective g-factor and is given by

$$g^{\mathrm{eff},\mu}_{n,n}(k) = g_0 \sigma^{\mu}_{n\rho,n\rho'}(k) + \frac{2\mathrm{i}}{m}\varepsilon_{\alpha\beta\mu} \sum_{\substack{m,\rho'\\ m\neq n}} \frac{\pi^{\alpha}_{n\rho,m\rho'}\pi^{\beta}_{m\rho',n\rho}}{E_{mn}}. \tag{2.2}$$

Here g_0 is the free-electron g-factor; $\boldsymbol{\sigma}$ are Pauli spin matrices; $\boldsymbol{\pi}$ are the momentum operators in the presence of spin–orbit interaction; n and m are band indices and the ρ are spin indices; $E_{mn} = E_m(k) - E_n(k)$; $\varepsilon_{\alpha\beta\mu}$ is an antisymmetric tensor of third rank; and we follow Einstein summation convention. In the absence of spin–orbit interactions, the second term becomes zero, and the effective g-factor reduces to the free-electron g-factor g_0. The matrix elements are taken between the periodic parts of the Bloch functions, and in general represented by

$$O^{\alpha}_{n\rho,m\rho'} = \int u^{*}_{nk\rho} O^{\alpha}(r) u_{mk\rho'} \mathrm{d}^3 r. \tag{2.3}$$

In PbTe, the energy surfaces at the L point are approximately prolate spheroids with the major axes in [111] directions. Therefore, within the first Brillouin zone, there are eight half-spheroids, or equivalently four complete spheroidal energy surfaces. However, the spheroidal approximation is only good for low carrier concentrations. With k vectors away from the band edge, the surfaces of constant energy become cylindrical. In the absence of a magnetic field, all the four valleys at $\langle 111\rangle$ zone edges are equivalent. However, in an arbitrary oriented external magnetic field, neither the matrix elements of $\boldsymbol{\sigma}$ nor the Fermi population factors are identical in the four valleys at the $\langle 111\rangle$ zone edges. However, when the field is applied along the [001] direction,

all the four valleys are equivalent. Following Mitchell and Wallis (1969), the crystallographic axes are taken along $X = [\bar{1}\bar{1}2]$, $Y = [1\bar{1}0]$ and $Z = [111]$. Thus, K can be written as

$$K = 4(\tfrac{1}{3}K^l + \tfrac{2}{3}K^t) \tag{2.4}$$

where the factor 4 comes about because of the four valleys, and K^l is the longitudinal component along [111] and K^t is the transverse component along $[\bar{1}\bar{1}2]$. Assuming the hyperfine matrix elements to be isotropic, we can write

$$g = \tfrac{1}{3}g^l + \tfrac{2}{3}g^t \tag{2.5}$$

where

$$g^l_{n\rho,n\rho'}(\boldsymbol{k}) = g_0\sigma^z_{n\rho,n\rho'} + \frac{2\mathrm{i}}{m}\sum_{\substack{m,\rho''\\ m\neq n}}\left(\frac{\pi^x_{n\rho,m\rho''}\pi^y_{m\rho'',n\rho'} - \pi^y_{n\rho,m\rho''}\pi^x_{m\rho'',n\rho'}}{E_{mn}}\right) \tag{2.6}$$

and

$$g^t_{n\rho,n\rho'}(\boldsymbol{k}) = g_0\sigma^x_{n\rho,n\rho'} + \frac{2\mathrm{i}}{m}\sum_{\substack{m,\rho''\\ m\neq n}}\left(\frac{\pi^y_{n\rho',m\rho''}\pi^z_{m\rho'',n\rho'} - \pi^z_{n\rho,m\rho''}\pi^y_{m\rho'',n\rho'}}{E_{mn}}\right). \tag{2.7}$$

3. Electronic structure

3.1. Background

The IV–VI semiconductors, which include the lead salts (PbS, PbSe and PbTe), are among the most interesting materials in solid-state physics (Cohen and Chelikowsky 1989). The above statement is justified for the fact that, despite their simple crystal structure (NaCl), some of these compounds exhibit ferroelectric, paraelectric and superconducting behaviour. Moreover, the temperature dependence of the energy gaps, the high value of static dielectric constants and the electronic structure of some of the alloys of these compounds appear to be anomalous compared to the conventional behaviour of the diamond and zincblende semiconductors.

PbTe and SnTe are considered as prototypes for this group and studies of these semiconductors are used to illustrate common features. The electronic structures of PbTe and SnTe and other compounds have been extensively investigated, both theoretically and experimentally. A variety of band calculations such as the relativistic augmented plane-waves (RAPW) method (Conklin *et al* 1965, Rabii and Lasseter 1969, Rabii 1969), the orthogonalized plane-wave (OPW) method (Herman *et al* 1968), the empirical pseudopotential method (Tung and Cohen 1969, Bernick and Kleinman 1970, Kohn *et al* 1973, Martinez *et al* 1975) and the relativistic Green function or Korringa–Kohn–Rostoker (KKR) method (Overhof and Rossler 1970) have been performed for these materials. More recently, a self-consistent RAPW calculation for SnTe (Melvin and Hendry 1979) and a first-principles pseudopotential total-energy calculation for the ground-state properties and electronic structures of PbTe and SnTe (Rabe and Joannopoulos 1985) have been reported. Although there is general agreement among the calculations on the energy levels and their spacings, the results do differ in detail. Thus, the finer features of the band structures for this group of compounds are not as well understood as in the case of the diamond and zincblende structures. Many of the existing

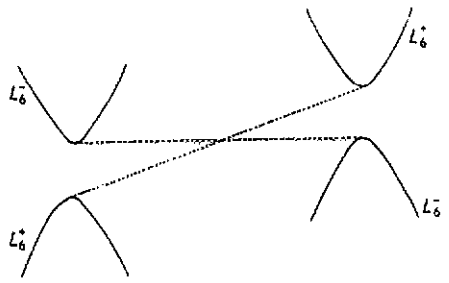

Figure 1. Band picture of $Pb_{1-x}Sn_xTe$ as a function of tin concentration.

Table 1. L-point basis functions and energy levels.

MW basis functions: only one of the Kramers conjugate pairs for each level is given	Energy levels	Magnitudes (Bernick and Kleinman) (2 Ryd)
$L_{61}^-\alpha = \cos\theta^- z\uparrow - \sin\theta^- x_+\downarrow$	ε_1^-	0.049
$L_5^-\alpha = (1/\sqrt{2})(-x_-\downarrow + ix_+\uparrow)$	ε_3^-	0.047
$L_{62}^-\alpha = \sin\theta^- z\uparrow + \cos\theta^- x_+\downarrow$	ε_2^-	0.007
$L_{61}^+\alpha = -i\cos\theta^+ R\uparrow - \sin\theta^+ S_+\downarrow$	ε_1^+	0.0
$L_5^+\alpha = (1/\sqrt{2})(S_-\downarrow + iS_+\uparrow)$	ε_3^+	−0.029
$L_{62}^+\alpha = i\sin\theta^+ R\uparrow + \cos\theta^+ S_+\downarrow$	ε_2^+	−0.049

band-structure calculations have some empirical input, and self-consistent methods have not yet been actively applied to this area. Thus calculations of physical quantities like the Knight shift (K), magnetic susceptibility and effective g-factors give adequate insight about the electronic structure of these materials.

The minimum energy gaps in both PbTe and SnTe occur at the L point of the Brillouin zone. The conduction and valence band edges have L_6^- and L_6^+ symmetry in the lead salts, but the ordering is reversed in the case of SnTe. Thus, the alloying of SnTe with PbTe causes a gradual variation of the energy gap as a function of composition. It has been established that the conduction and valence bands actually cross at a critical composition, and this band inversion composition is somewhat temperature-dependent. A schematic picture of this crossing is shown in figure 1. In addition to the band-edge levels, two more bands on each side of the energy gap are of importance for the interpretation of physical properties. The basis functions and corresponding energy levels in order from the top of the conduction band to the bottom of the valence band in the Mitchell and Wallis (MW) (1966) notation are given in table 1. We follow the Bernick and Kleinman (1970) band ordering.

In table 1, $\cos\theta^{\pm}$ and $\sin\theta^{\pm}$ are the amplitudes of single-group functions in the double-group basis functions. The spatial parts of the basis functions have the following transformation properties about Pb: R transforms like an atomic s state, $x_{\pm}$ and z transform like atomic p functions with $m_z = \pm 1$ and 0, and $S_{\pm}$ transform like atomic d functions with $m_z = \pm 1$.

3.2. Six-level $k \cdot \pi$ theory

We consider the eigenvalue equation

$$[\pi^2/2m + V(r)]\chi(k, r) = E\chi(k, r) \tag{3.1}$$

where $\chi(k, r)$ are the Luttinger and Kohn (1955) wavefunctions

$$\chi(k, r) = \sum_n C_n(k)\, e^{i(k-k_0)\cdot r}\psi_{nk_0}(r). \tag{3.2}$$

Here $\psi_{nk_0}(r)$ is the Bloch function at k_0:

$$\psi_{nk_0}(r) = e^{ik_0\cdot r}U_{nk_0}(r). \tag{3.3}$$

Using equations (3.2) and (3.3) in equation (3.1), multiplying both sides of equation (3.1) on the left by $u^*_{n'k_0}(r)$ and integrating over the whole space, we obtain

$$\sum_n \left[\left(E_{nk_0} + \frac{\hbar}{2m}(k^2 - k_0^2) - E\right)\delta_{nn'} + \frac{\hbar}{m}(k - k_0)\cdot\pi_{nn'}\right] C_n = 0 \tag{3.4}$$

where

$$\pi_{nn'} = \int_{\text{cell}} u^*_{nk_0\rho}(r)\pi u_{n'k_0\rho'}(r)\, d^3r. \tag{3.5}$$

The integral in equation (3.5) is over the unit cell. Let us assume that k_0 is the L point in the Brillouin zone. Referring to this point as the origin in k-space, we write equation (3.4) as

$$\sum_n \left[\left(E_{nk_0} + \frac{\hbar^2k^2}{2m} - E\right)\delta_{nn'} + \frac{\hbar}{m}(k\cdot\pi)_{nn'}\right] C_n = 0. \tag{3.6}$$

Equation (3.6) gives a complete description of energy bands throughout k-space in terms of energy E_{nk_0} and momentum matrix elements $\pi_{nn'}$. This is the basic equation of the $k \cdot \pi$ representation.

In PbTe, there are six levels around the energy gap that contribute significantly to a $k \cdot \pi$ perturbation theory. The band-edge levels according to Bernick–Kleinman ordering ($L^-_{62}\alpha$, $L^-_{62}\beta$, $L^+_{61}\alpha$ and $L^+_{61}\beta$) are diagonalized exactly and the interaction with other bands is treated up to second order.

The diagonalization of the band-edge states gives the wavefunctions

$$\psi_1 = \left(\frac{1+w}{2w}\right)^{1/2} L^-_{62}\alpha - \frac{\sqrt{2}(\hbar/m)tk_z}{E_G[w(1+w)]^{1/2}} L^+_{61}\alpha + \frac{\sqrt{2}(\hbar/m)sk_+}{E_G[w(1+w)]^{1/2}} L^+_{61}\beta \tag{3.7a}$$

$$\psi_2 = \left(\frac{1+w}{2w}\right)^{1/2} L^-_{62}\beta + \frac{\sqrt{2}(\hbar/m)tk_z}{E_G[w(1+w)]^{1/2}} L^+_{61}\beta + \frac{\sqrt{2}(\hbar/m)sk_-}{E_G[w(1+w)]^{1/2}} L^+_{61}\alpha \tag{3.7b}$$

$$\psi_3 = \left(\frac{1+w}{2w}\right)^{1/2} L^+_{61}\alpha + \frac{\sqrt{2}(\hbar/m)tk_z}{E_G[w(1+w)]^{1/2}} L^-_{62}\alpha - \frac{\sqrt{2}(\hbar/m)sk_+}{E_G[w(1+w)]^{1/2}} L^-_{62}\beta \tag{3.7c}$$

$$\psi_4 = \left(\frac{1+w}{2w}\right)^{1/2} L_{61}^{+}\beta - \frac{\sqrt{2}(\hbar/m)tk_z}{E_G[w(1+w)]^{1/2}} L_{62}^{-}\beta - \frac{\sqrt{2}(\hbar/m)sk_-}{E_G[w(1+w)]^{1/2}} L_{62}^{-}\alpha \tag{3.7d}$$

and the energies

$$E_2^- = \varepsilon_2^- + \hbar^2k^2/2m + \tfrac{1}{2}E_G(w-1) \tag{3.8a}$$

$$E_1^+ = \varepsilon_1^+ + \hbar^2k^2/2m - \tfrac{1}{2}E_G(w-1). \tag{3.8b}$$

In equations (3.7) and (3.8),

$$w = \left(1 + 2\frac{\hbar^2}{m^2}\frac{s^2k_\rho^2}{E_G^2} + 4\frac{\hbar^2}{m^2}\frac{t^2k_z^2}{E_G^2}\right)^{1/2} \tag{3.9}$$

$$s = \langle L_{61}^{+}\alpha|\pi^{+}|L_{62}^{-}\beta\rangle = \langle L_{61}^{+}\beta|\pi^{-}|L_{62}^{-}\alpha\rangle \tag{3.10}$$

$$t = -\langle L_{61}^{+}\alpha|\pi^{z}|L_{62}^{-}\alpha\rangle = \langle L_{61}^{+}\beta|\pi^{z}|L_{62}^{-}\beta\rangle \tag{3.11}$$

$$k_\rho^2 = k_x^2 + k_y^2 \tag{3.12}$$

$$k_\pm = (k_x \pm ik_y)/\sqrt{2} \tag{3.13}$$

$$\pi^\pm = (\pi^x \pm i\pi^y)/\sqrt{2}. \tag{3.14}$$

The interaction between band-edge states has so far been considered. Interaction of far bands has been considered up to second order in perturbation theory and the result is

$$\begin{aligned} E_{c,v}(k) = {} & \varepsilon_{c,v} + \hbar^2k^2/2m \pm \tfrac{1}{2}E_G(w-1) + M_{1c,v}k_\rho^2 + M_{2c,v}k_z^2 \\ & + [M_{3c,v}/w(1+w) + M_{4c,v}/w]k_\rho^4 + [M_{5c,v}/w(1+w) + M_{6c,v}/w]k_z^4 \\ & + [M_{7c,v}/w(1+w) + M_{8c,v}/w]k_\rho^2k_z^2 \end{aligned} \tag{3.15}$$

where the suffixes c and v denote the conduction and valence bands except in the third term in which case these are denoted by + and − signs. M_1 to M_8 are complicated functions of momentum matrix elements and energy gaps at the L point (Misra *et al* 1984). The chemical potential is calculated, using a self-consistent method, from the following expression:

$$\mu = \mu_0 + [\mu - (\hbar^2/2m)(3\pi^2F)^{2/3}] \tag{3.16}$$

where

$$F = \frac{8}{(2\pi)^3}\int f(E_{c,v}(k) - \mu)\,\mathrm{d}^3k \tag{3.17}$$

and

$$\mu_0 = (\hbar^2/2m)(3\pi^2n)^{2/3}. \tag{3.18}$$

The factor 8 in equation (3.17) accounts for the spin degeneracies of the energy levels and the four L valleys of the Brillouin zone; μ_0 is the free-electron chemical potential and n is the carrier density. We use cylindrical coordinates for the evaluation of equation

Table 2. Matrix elements of $k \cdot \pi$.

$k \cdot \pi$	$L_{61}^{-}\alpha$	$L_{61}^{-}\beta$	$L_{62}^{-}\beta$	$L_{62}^{-}\alpha$	$L_{4}^{-}\beta$	$L_{5}^{-}\alpha$
$L_{61}^{+}\alpha$	$-Ek_z$	Bk_-	sk_-	$-tk_z$	Hk_+	iH^*k_+
$L_{61}^{+}\beta$	Bk_+	Ek_z	tk_z	sk_+	iHk_-	H^*k_-
$L_{62}^{+}\beta$	Dk_+	Fk_z	fk_z	dk_+	iJk_-	J^*k_-
$L_{62}^{+}\alpha$	$-Fk_z$	Dk_-	dk_-	fk_z	Jk_+	iJ^*k_+
$L_{4}^{+}\beta$	Ak_-	$-iAk_+$	$-iak_+$	ak_-	0	$-Lk_z$
$L_{5}^{+}\alpha$	$-iA^*k_-$	A^*k_+	a^*k_+	$-ia^*k_-$	Lk_z	0

(3.17) and the integration is done numerically. The variation of the energy gap with temperature and tin concentration is considered using the formula (Dimmock *et al* 1966)

$$E_G(x, T) = |E_G(0, T) - 0.543x + 0.02x^2| \text{ eV} \tag{3.19}$$

where $E_G(0, T)$ represents the temperature dependence of PbTe energy gap and is given by

$$E_G(0, T) = E_G(0, 0) + 4.85 \times 10^{-4} T \text{ eV K}^{-1} \tag{3.20}$$

where T is the temperature in kelvins.

It was found that for a fixed carrier density the chemical potential decreases with increase in tin concentration.

4. Results and discussion

In order to evaluate the g-factors we need to know the momentum matrix elements. We give the matrix elements of $k \cdot \pi$ between the double-group basis functions at the L point in table 2 (Mitchell and Wallis 1969).

In table 2, the constants used are

$$\begin{aligned}
s &= -\sin\theta^+ \sin\theta^- P_{31} - \cos\theta^+ \cos\theta^- P_{13} \\
a &= (1/\sqrt{2}) \sin\theta^- P_{31} + i \cos\theta^- P_{22} \\
d &= \sin\theta^- \cos\theta^- P_{31} - \sin\theta^+ \cos\theta^+ P_{13} \\
t &= \sin\theta^- \cos\theta^+ P_{11} + \cos\theta^- \sin\theta^+ P_{21} \\
f &= -\sin\theta^- \sin\theta^+ P_{11} - \cos\theta^+ \cos\theta^- P_{21} \\
H &= (1/\sqrt{2}) \cos\theta^+ P_{13} + i \sin\theta^+ P_{22} \\
J &= (1/\sqrt{2}) \sin\theta^+ P_{13} + i \cos\theta^+ P_{22} \\
L &= i P_{21} \\
B &= \cos\theta^+ \sin\theta^- P_{13} - \cos\theta^- \sin\theta^+ P_{31} \\
A &= (1/\sqrt{2}) \cos\theta^+ P_{31} - i \sin\theta^- P_{22} \\
D &= \cos\theta^+ \cos\theta^- P_{31} + \sin\theta^+ \sin\theta^- P_{13}
\end{aligned} \tag{4.1}$$

Table 3. Details of g-factor results in $Pb_{1-x}Sn_xTe$.

Carrier density	Tin concentration, x	Temperature (K)	g' (calc.)	g' (calc.)	g' (exp.[a])	g' (exp.[a])	g (theor.)	g (exp.[a])
Valence band edge	0	4.2	49.21	13.64	51 ± 8		25.5	
Band edge	0.09	47	60.64	16.55			31.25	56
Band edge	0.09	97	52.68	14.52			27.24	38
Band edge	0.16	47	82.17	22.03			42.08	69
Band edge	0.19	4.2	116.67	30.81			59.43	77
Band edge	0.21	4.2	133.81	35.17			68.05	84
Band edge	0.26	4.2	207.10	53.83			104.92	112
Band edge	0.27	4.2	231.69	60.08			117.29	120
$p = 3.0 \times 10^{18}$ cm^{-3}	0	0	42.07	9.14	32 ± 2	7 ± 2	20.12	
$p = 3.5 \times 10^{18}$ cm^{-3}	0	0	41.49	8.79	30.0	10	19.69	
Conduction band edge	0	4.2	48.94	14.22	45 ± 8	15 ± 1	25.79	
$n = 8 \times 10^{16}$ cm^{-3}	0	0	48.40	13.70	57 ± 5	15 ± 1	25.27	

[a] Hewes *et al* (1973).

$$E = -\cos\theta^+ \cos\theta^- P_{31} + \sin\theta^+ \sin\theta^- P_{21}$$

$$F = -\cos\theta^- \sin\theta^+ P_{11} + \sin\theta^- \cos\theta^+ P_{21}.$$

In equations (4.1), $P_{11}, P_{21}, P_{31}, P_{22}$ and P_{13} are the momentum matrix elements between the single-group states (Mitchell and Wallis 1969).

For the conduction band g-factor, we have, using equation (2.6),

$$g_c^l = g_0\langle\psi_1|\sigma^z|\psi_1\rangle + \frac{2i}{m}\sum_{\substack{m,\rho''\\ m\neq n}}\left(\frac{\langle\psi_1|\pi^x|m\rho''\rangle\langle m\rho''|\pi^y|\psi_1\rangle - \langle\psi_1|\pi^y|m\rho''\rangle\langle m\rho''|\pi^x|\psi_1\rangle}{E_m - E_2^-}\right) \tag{4.2}$$

and

$$g_c^l = g_0\langle\psi_1|\sigma^x|\psi_2\rangle + \frac{2i}{m}\sum_{\substack{m,\rho''\\ m\neq n}}\left(\frac{\langle\psi_1|\pi^y|m\rho''\rangle\langle m\rho''|\pi^z|\psi_2\rangle - \langle\psi_1|\pi^z|m\rho''\rangle\langle m\rho''|\pi^y|\psi_2\rangle}{E_m - E_2^-}\right) \tag{4.3}$$

where m takes all other energy levels except the energy levels represented by ψ_1 and ψ_2.

From equations (3.7), (3.8), (3.13) and (4.1) to (4.3), and table 2, we can write

$$\begin{aligned} g_c^l = g_0\Bigg[&-\left(\frac{1+w}{2w}\right)\cos 2\theta^- + \frac{\hbar^2\cos 2\theta^+}{m^2E_G^2w(1+w)}(2t^2k_z^2 - s^2k_\rho^2)\Bigg] \\ &+ \frac{2}{m}\Bigg\{\Bigg[\left(\frac{1+w}{2w}s + \frac{2\hbar^2t^2sk_z^2}{m^2E_G^2w(1+w)}\right)^2 - \frac{\hbar^4}{m^4}\frac{s^6k_\rho^4}{E_G^4w^2(1+w)^2}\Bigg]\frac{1}{E_Gw} \\ &+ 2\left(\frac{1+w}{2w}\right)\left(\frac{2|a|^2}{2(\varepsilon_3^+ - \varepsilon_2^-) - E_G(w-1)} - \frac{d^2}{2(\varepsilon_2^+ - \varepsilon_2^-) - E_G(w-1)}\right) \\ &+ \frac{2\hbar^2(s^2k_\rho^2 - 2t^2k_z^2)}{m^2E_G^2w(1+w)} \\ &\times\left(\frac{B^2}{2(\varepsilon_1^- - \varepsilon_2^-) - E_G(w-1)} - \frac{2|H|^2}{2(\varepsilon_3^- - \varepsilon_2^-) - E_G(w-1)}\right)\Bigg\} \end{aligned} \tag{4.4}$$

and

$$\begin{aligned} g_c^t = g_0\Bigg[&\left(\frac{1+w}{2w}\right)\sin^2\theta^- + \frac{\hbar^2\cos^2\theta^+}{m^2E_G^2w(1+w)}(2t^2k_z^2 - s^2k_\rho^2)\Bigg] \\ &+ \frac{2\sqrt{2}}{m}\Bigg[-\frac{st}{E_Gw} + \frac{4\hbar^2t^3sk_z^2}{m^2E_G^3w^2(1+w)} \\ &+ \frac{2\hbar^2BE(s^2k_\rho^2 - 2t^2k_z^2)}{m^2E_G^2w(1+w)[2(\varepsilon_1^- - \varepsilon_2^-) - E_G(w-1)]} \\ &+ \left(\frac{1+w}{2w}\right)\frac{2df}{2(\varepsilon_2^+ - \varepsilon_2^-) - E_G(w-1)}\Bigg]. \end{aligned} \tag{4.5}$$

In the band-edge limit, i.e. when $k_\rho^2 = 0$ and $k_z = 0$, our results reduce to the Mitchell

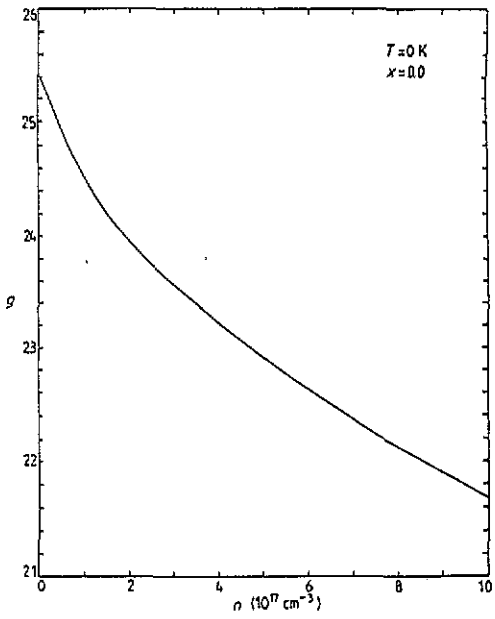

Figure 2. Effective g-factor versus carrier concentration for n-type PbTe.

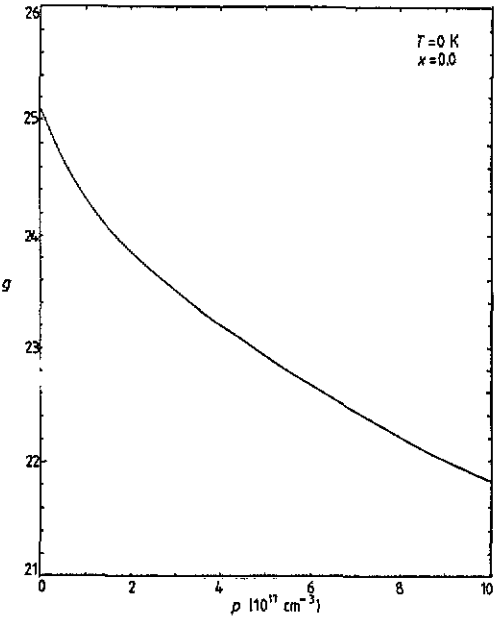

Figure 3. Effective g-factor versus carrier concentration for p-type PbTe.

and Wallis (1969) expressions. The g-values were calculated by substituting k_z by its Fermi surface value k_f, which is obtained by solving the equation

$$E_c(k_\rho^2, k_f) - \mu = 0 \tag{4.6}$$

for $k_\rho^2 = 0$. The single-group momentum matrix elements, the amplitudes of single groups in the double-group eigenfunctions and the energy levels were obtained from Bernick and Kleinman (1970). The valence band g-factors were obtained from equations (4.4) and (4.5) by the following exchanges: $d \leftrightarrow B$, $a \leftrightarrow H$, $f \leftrightarrow E$, $J \leftrightarrow A$ and $L = -L$ for the matrix elements, and $\varepsilon_2^- \leftrightarrow \varepsilon_1^+$, $\varepsilon_3^- \leftrightarrow \varepsilon_3^+$, $\varepsilon_1^- \leftrightarrow \varepsilon_2^+$ and $E_G = -E_G$ for the energy levels.

We have plotted the g-values versus carrier density for both n- and p-type PbTe in figures 2 and 3. It is seen that the g-values decrease with increase in carrier concentration. In figures 4 and 5 we have plotted the g-values for n- and p-type $Pb_{1-x}Sn_xTe$, respectively, as functions of temperature for two typical values of carrier concentrations and tin concentrations. We found that for fixed carrier concentrations and tin concentrations, g-values decrease with temperature. For fixed carrier density and temperature, however, g-values increase with increase in tin concentration (figures 6 and 7). Our results are compared with experiment where available in table 3. The agreement between our results and experiment is, except in a couple of cases, good to excellent. It may be noted that Hewes *et al* (1973) have obtained better agreement than us. However, their results were obtained by using several parameters obtained from experiment. On the other hand, ours is the first *ab initio* calculation for the g-factors as functions of carrier density, tin concentration and temperature.

We have seen that the transverse g-factors change sign by changing the sign of $\sin\theta^{\pm}$, which does not change the energy levels, as has been discussed earlier (Tripathi *et al*

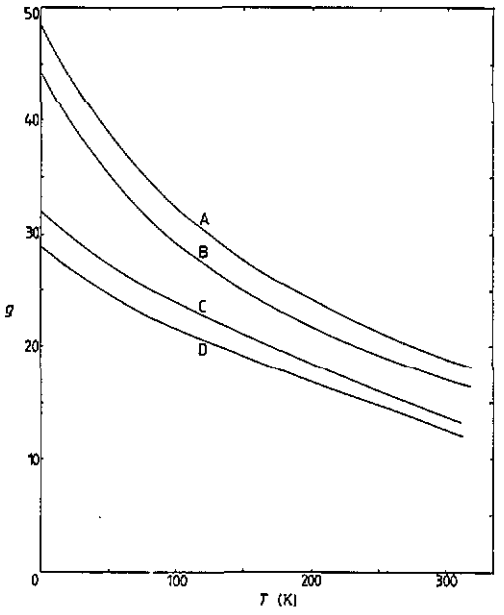

Figure 4. Effective g-factor versus temperature for two typical values of carrier (electron) and tin concentrations. A: $n = 3.0 \times 10^{17}\,cm^{-3}, x = 0.16$; B: $n = 1.2 \times 10^{18}\ cm^{-3}$, $x = 0.16$; C: $n = 3.0 \times 10^{17}\,cm^{-3}, x = 0.08$; D: $n = 1.2 \times 10^{18}\,cm^{-3}$, $x = 0.08$.

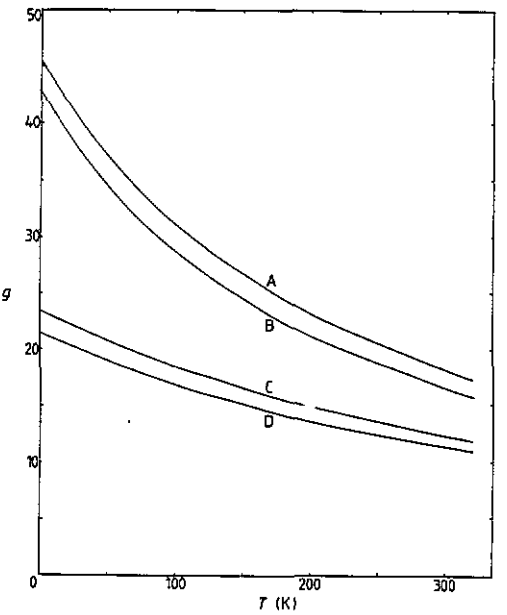

Figure 5. Effective g-factor versus temperature for two typical values of carrier (hole) and tin concentrations. A: $p = 3.0 \times 10^{17}\,cm^{-3}, x = 0.15$; B: $p = 1.2 \times 10^{18}\ cm^{-3}$, $x = 0.15$; C: $p = 3.0 \times 10^{17}\,cm^{-3}, x = 0.00$; D: $p = 1.2 \times 10^{18}\,cm^{-3}$, $x = 0.00$.

1981, 1982). Thus, we believe that the sign of the g-factor is not unique, as is the case in the Knight shift. Our results can be improved by the following methods. We consider a virtual crystal approximation, which is only good for low concentration of tin. More realistic calculations valid for an alloy system should be considered, as has been done in the electronic structure calculation of $Pb_{1-x}Sn_xTe$ (Lee and Dow 1987). We have considered exact diagonalization of band-edge states only and the far bands are taken into account through second-order perturbation. This should be improved for the results to be valid for carrier densities beyond the limit of about $10^{18}\,cm^{-3}$.

5. Summary and conclusions

In this work, we have made a careful analysis of the effective g-factors in $Pb_{1-x}Sn_xTe$. This work presents, to our knowledge, the first *ab initio* calculation of effective g-factors as functions of carrier density, tin concentration and temperature. The formulation is general and can be applied to the other ternary compound, $Pb_{1-x}Ge_xTe$, of this family. We have not done this, because of the unavailability of data for the variation of the temperature-dependent energy gap as a function of Ge concentration. Except in a couple of cases, our results agree fairly well with experiment where available. Also, the overall trends and results obtained are in general conformity with the experimental results.

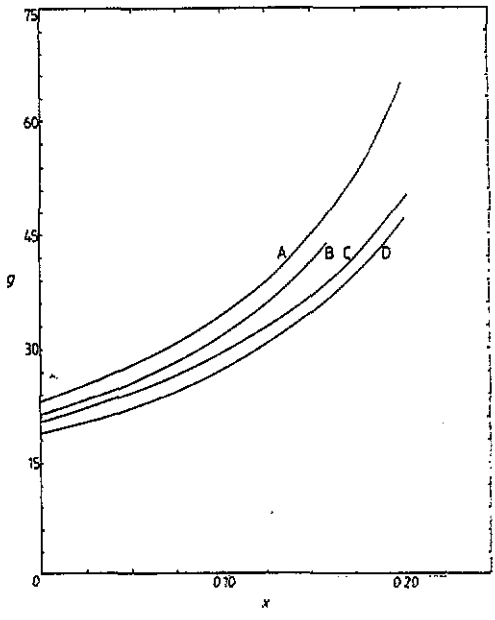

Figure 6. Effective g-factor versus tin concentration for two typical values of carrier (electron) concentration and temperature. A: $n = 3.0 \times 10^{17}\,cm^{-3}$, $T = 0$ K; B: $n = 1.2 \times 10^{18}\,cm^{-3}$, $T = 0$ K; C: $n = 3.0 \times 10^{17}\,cm^{-3}$, $T = 50$ K; D: $n = 1.2 \times 10^{18}\,cm^{-3}$, $T = 50$ K.

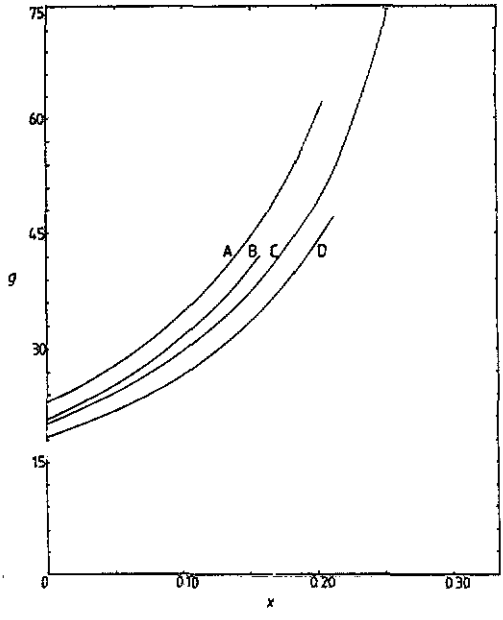

Figure 7. Effective g-factor versus tin concentration for two typical values of carrier (hole) concentration and temperature. A: $p = 3.0 \times 10^{17}\,cm^{-3}$, $T = 0$ K; B: $p = 1.2 \times 10^{18}\,cm^{-3}$, $T = 0$ K; C: $p = 3.0 \times 10^{17}\,cm^{-3}$, $T = 50$ K; D: $p = 1.2 \times 10^{18}\,cm^{-3}$, $T = 50$ K.

The formulation can suitably be applied to study the enhancement of g-factors in semimagnetic semiconductors, such as $Pb_{1-x}Mn_xTe$ and $Pb_{1-x}Fe_xTe$. However, the g-factor expressions should include the effects of s–d and s–f hybridizations, as has been incorporated in the case of the Knight shift (Tripathi 1985, Tripathi *et al* 1987). Such a formulation is in progress and results will be reported when available.

Acknowledgment

The research was supported by the University Grants Commission (India) through a research grant.

References

Bastard G, Rigaux C, Guldner Y, Mycielski A, Furdyna J K and Mullin D P 1981 *Phys. Rev.* B **24** 1961
Bernick R L and Kleinman L 1970 *Solid State Commun.* **8** 569
Cohen M L and Chelikowsky J R 1989 *Electronic Structure and Optical Properties of Semiconductors* (Heidelberg: Springer) p 172
Conklin J B, Johnson L E and Pratt G W 1965 *Phys. Rev.* **137** A1282
deCastro A R B and Schumacher R T 1973 *Phys. Rev.* B **7** 105
Dimmock J O, Melngailis I and Strauss A J 1966 *Phys. Rev. Lett.* **16** 1193
Dobrowolska M, Dobrowolski W, Galazka R R and Mycielski A 1981 *Phys. Status Solidi* b **105** 477
Dobrowolski W, Von Ortenberg M, Thielman J and Galazka R R 1981 *Phys. Rev. Lett.* **47** 541

Heiman D, Wolff P A and Warnock J 1983 *Phys. Rev.* B **27** 4848
Herman F, Kortum L, Ortenberg I B and Van Dyke J P 1968 *J. Physique Coll.* **29** C4, 62
Hewes C R, Adler M S and Senturia S D 1973 *Phys. Rev.* B **7** 5195
Hota R L and Tripathi G S 1990 *Solid State Phys (India)* **33C** 344; 1991 *Phys. Rev.* B at press
Kohn S E, Yu P Y, Petroff Y R, Shen R, Tsang Y and Cohen M L 1973 *Phys. Rev.* B **8** 1477
Lee S and Dow J D 1987 *Phys. Rev.* B **36** 5968
Leloup J Y and Sapoval B 1979 *Phys. Status Solidi* b **91** 427
Leloup J Y, Sapoval B and Martinez G 1973 *Phys. Rev.* B **7** 5276
Luttinger J M and Kohn W 1955 *Phys. Rev.* **97** 869
Martinez G, Schlutter M and Cohen M L 1975 *Phys. Rev.* B **11** 651
Melvin J S and Hendry D C 1979 *J. Phys. C: Solid State Phys.* **12** 3003
Misra C M and Tripathi G S 1989 *Phys. Rev.* B **40** 11168
Misra P K and Kleinman L 1972 *Phys. Rev.* B **5** 4581
Misra S, Tripathi G S and Misra P K 1984 *J. Phys. C: Solid State Phys.* **17** 869
—— 1985 *Phys. Lett.* **110A** 461
—— 1986 *J. Phys. C: Solid State Phys.* **19** 2007
—— 1987 *J. Phys. C: Solid State Phys.* **20** 277
Mitchell D L and Wallis R F 1966 *Phys. Rev.* **151** 581
Overhof H and Rossler U 1970 *Phys. Status Solidi* b **37** 691
Rabe K M and Joanopoulos J D 1985 *Phys. Rev.* B **32** 2302
Rabii S 1969 *Phys. Rev.* **182** 821
Rabii S and Lasseter R H 1969 *Phys. Rev. Lett.* **33** 703
Roth L M 1960 *Phys. Rev.* **188** 1534
Sapoval B and Leloup J Y 1973 *Phys. Rev.* B **7** 5272
Tripathi G S 1985 *J. Phys. C: Solid State Phys.* **18** L1157
Tripathi G S, Das L K, Misra P K and Mahanti S D 1981 *Solid State Commun.* **38** 1207
—— 1982 *Phys. Rev.* B **25** 3209
Tripathi G S, Mishra B and Misra P K 1987 *J. Magn. Magn. Mater.* **67** 271
Tung Y W and Cohen M L 1969 *Phys. Rev.* **180** 823
Yafet Y 1963 *Solid State Phys.* **14** 1